Live-imaging of revertant and therapeutically restored dystrophin in the *Dmd*^{*EGFP-mdx*} mouse model for Duchenne muscular dystrophy

M. V. Petkova*†,[1] , A. Stantzou*,[1] , A. Morin* , O. Petrova* , S. Morales-Gonzalez†,
F. Seifert†, J. Bellec-Dyevre‡, T. Manoliu§ , A. Goyenvalle*¶ , L. Garcia*¶, I. Richard‡ ,
C. Laplace-Builhé§ , M. Schuelke† and H. Amthor***

*Université Paris-Saclay, UVSQ, Inserm, END-ICAP, Versailles, France, † Department of Neuropediatrics, Charité–Universitätsmedizin Berlin, corporate member of Freie Universität Berlin, Humboldt-Universität zu Berlin, Berlin Institute of Health (BIH), NeuroCure Clinical Research Center, Berlin, Germany, ‡Integrare (UMR_S951), Inserm, Généthon, Univ Evry, Université Paris-Saclay, Evry, France, §Gustave Roussy, Université Paris-Saclay, Plate-forme Imagerie et Cytométrie., UMS AMMCa., Villejuif, France, ¶LIA BAHN, Centre scientifique de Monaco, Monaco and **Pediatric Department, University Hospital Raymond Poincaré, Garches, France*

Background: *Dmd*^{*mdx*}, harbouring the c.2983C>T nonsense mutation in *Dmd* exon 23, is a mouse model for Duchenne muscular dystrophy (DMD), frequently used to test therapies aimed at dystrophin restoration. Current translational research is methodologically hampered by the lack of a reporter mouse model, which would allow direct visualization of dystrophin expression as well as longitudinal *in vivo* studies. **Methods**: We generated a *Dmd*^{*EGFP-mdx*} reporter allele carrying in *cis* the *mdx*-23 mutation and a C-terminal EGFP-tag. This mouse model allows direct visualization of spontaneously and therapeutically restored dystrophin-EGFP fusion protein either after natural fibre reversion, or for example, after splice modulation using tricyclo-DNA to skip *Dmd* exon 23, or after gene editing using AAV-encoded CRISPR/Cas9 for *Dmd* exon 23 excision. **Results**: Intravital microscopy in anaesthetized mice allowed live-imaging of sarcolemmal dystrophin-EGFP fusion protein of revertant fibres as well as following therapeutic restoration. Dystrophin-EGFP-fluorescence persisted *ex vivo*, allowing live-imaging of revertant and therapeutically restored dystrophin in isolated fibres *ex vivo*. Expression of the shorter dystrophin-EGFP isoforms Dp71 in the brain, Dp260 in the retina, and Dp116 in the peripheral nerve remained unabated by the *mdx*-23 mutation. **Conclusion**: Intravital imaging of *Dmd*^{*EGFP-mdx*} muscle permits novel experimental approaches such as the study of revertant and therapeutically restored dystrophin *in vivo* and *ex vivo*.

Keywords: CRISPR/Cas9, Duchenne muscular dystrophy, dystrophin-EGFP fusion protein, *mdx* reporter mouse model, revertant muscle fibre, tcDNA

Correspondence: Markus Schuelke MD, Klinik für Pädiatrie m. S. Neurolgie, Charité-Universitätsmedizin Berlin, Augustenburger Platz 1, 13353 Berlin, Phone +49 30 4505 66112, FAX +49 30 4505 66920, email: markus.schuelke@charite.de
Helge Amthor MD PhD, laboratoire U1179, UFR Simone Veil - Santé, 2 avenue de la Source de la Bièvre, 78180 Montigny-le-Bretonneux, France, Phone +33 1 70 42 92 29, email: helge.amthor@uvsq.fr

[1]*Equally contributed.

Introduction

The X-chromosome-linked muscular dystrophy (*mdx*) mouse is the most frequently used animal model in preclinical research for Duchenne muscular dystrophy (DMD), a devastating and the most frequent muscle disease of childhood. The classical *mdx* mouse, also referred to as *Dmd*^{mdx} mouse, carries a c.2983C>T nonsense mutation in exon 23 of the *Dmd* gene (also called the *mdx*-23 allele), resulting in a termination codon (TAA) in place of a glutamine codon (CAA) [1,2]. The mutation causes complete absence of the *Dmd*-encoded full-length dystrophin isoform Dp427, which in wild-type is expressed in skeletal, smooth, and cardiac muscle and in the central nervous system [1]. All other shorter dystrophin isoforms (Dp260, Dp140, Dp116, and Dp71) are transcribed from more distal promoters located downstream of *Dmd* exon 23 and are thus normally expressed in the *mdx* mouse model [2–5]. Of note, *Dmd* exon 23 is one of many exons that encode part of the core region of the dystrophin protein, and its removal would not shift the reading frame.

Indeed, the deletion or exclusion of the mutated *Dmd* exon 23 by alternative splicing restores the open reading frame and entails expression of truncated dystrophin products that ameliorate the pathological *mdx* phenotype [6–8]. Interestingly, in *mdx* mice, similarly to other DMD animal models as well as in human patients, some myofibres spontaneously overcome the null mutation [9]. Such so-called 'revertant fibres' express internally truncated dystrophin that excludes at least the *Dmd* exon 23 encoded protein domain [10]. The presence of a nonsense mutation in an 'in frame' exon makes *Dmd*^{mdx} an ideal animal model for testing therapeutic strategies that aim at restoring the function of the mutated *Dmd* gene. Such approaches would comprise (**i**) antisense-induced splice modulation to skip the mutated exon 23 during RNA maturation using antisense oligonucleotides (AON) such as tricyclo-DNA (tcDNA) [11], (**ii**) stop codon read-trough during translation, and (**iii**) CRISPR-Cas9-induced genomic deletion of *Dmd* exon 23 [12].

Hitherto, no *Dmd*^{mdx} reporter mouse models are available allowing the visualization of dystrophin re-expression in an otherwise dystrophin-negative background. Therefore, current imaging of restored dystrophin in *mdx* mice relies entirely on immunostaining. However, antibody-dependent protocols have several methodological limitations: (**i**) they do not allow intravital imaging or live-cell imaging in cell cultures; (**ii**) it is difficult to quantify signals due to antibody-mediated signal amplification; (**iii**) nonspecific immunostaining by cross-reacting antibodies is aggravated by the chronic inflammation and by antibody deposition in the *mdx* muscle, and (**iv**) using epitope specific anti-dystrophin antibodies, certain dystrophin isoforms might go undetected.

We recently generated the *Dmd*^{EGFP} reporter mouse line that allows localizing, tracing and analysing dystrophin *in* and *ex vivo* by means of native EGFP-fluorescence. We generated *Dmd*^{EGFP} mice through modification of the *Dmd* locus by in-frame insertion of a FLAG-EGFP sequence downstream of the last *Dmd* exon 79. The *Dmd*^{EGFP} reporter mice express a fluorescently labelled dystrophin-EGFP fusion protein from the endogenous locus, which does not interfere with normal dystrophin function [13]. *Dmd*^{EGFP} mice show strong native dystrophin-EGFP fluorescence in skeletal and smooth muscle, heart, brain, and the eye that co-localizes with known subcellular sites of dystrophin expression, suggesting proper tagging and distribution of the major dystrophin isoforms. Isolated myofibres and satellite cell-derived myotubes express dystrophin-EGFP *in vitro* [13].

Here we describe the generation of a novel dystrophin reporter mouse model by crossing the *Dmd*^{EGFP} allele into the *mdx* background in *cis*. The so generated *Dmd*^{EGFP-mdx} mice carry the *mdx* exon 23 nonsense mutation and the *EGFP* sequence on the same allele. We show that dystrophin-EGFP is re-expressed in the dystrophin-negative background of the *Dmd*^{EGFP-mdx} muscle (**i**) in revertant fibres, (**ii**) after therapeutic restoration of the dystrophin reading frame, and (**iii**) in tissues that express short dystrophin isoforms that are not affected by the *mdx*-23 mutation.

Materials and Methods

Generation and genotyping of transgenic mice

We conducted all animal experiments according to the National and European legislation as well as to institutional guidelines for the care and use of laboratory animals as approved by the local authorities (LaGeSo Berlin, T 0222/13) and approved by the French

government (Ministère de l'Enseignement Supérieur et de la Recherche, autorisation APAFiS).

To generate the $Dmd^{EGFP\text{-}mdx}$ mice, we crossed the Dmd^{EGFP} mouse line, previously generated in our laboratory on the C57BL/6N background [13], with the conventional Dmd^{mdx} (C57BL/10ScSn-Dmd^{mdx}/J) mouse line that had before been backcrossed into the C57BL6/N background for >9 generations [14]. We achieved our goal to introduce the Dmd^{EGFP} allele into the *mdx* background in *cis* through natural recombination during meiosis in female F1 mice that were heterozygous for both the Dmd^{EGFP} and the *mdx*-23 allele. We screened for successful crossing over in males of the F2 generation by genotyping. . From the F4 generation onward we were then able to breed the mice as homozygous/hemizygous $Dmd^{EGFP\text{-}mdx}$ strains.

Genotyping was performed on genomic DNA isolated from ear clippings. A three-primer PCR allowed the distinction between animals that were heterozygous or homozygous for the *EGFP* sequence using following primers: FW#1: 5′-TGA CTC CCA ATA GTG GCA ACC-3′, FW#2 5′-GAG CAA AGA CCC CAA CGA GA-3′, REV: 5′-CCA TGC GGG AAT CAG GAG TT-3′ (wild-type = 202 bp, Dmd^{EGFP} = 304 bp). Sanger sequencing was done to screen for the *mdx* mutation using oligonucleotide primers flanking the exon *mdx*-23 mutation (FW: 5′-AAC TCA AAT ATG CGT GTT AGT-3′, REV: 5′-CTC AAT CTC TTC AAA TTC TG-3′). Dmd^{EGFP} and $Dmd^{EGFP\text{-}mdx}$ mice were bred and maintained in a standard 12 h light/dark cycle and had *ad libitum* access to food and water. Mice were weaned at 4 weeks of age and were kept in small colonies of two to five animals per cage.

Antisense oligonucleotide treatment

The tcDNA-AON PS M23D 15-mer (+2-13) (5′-pAAC CTC GGC TTA CCT-3′) targeting the donor splice site of exon 23 *Dmd* pre-mRNA was synthesized by SYNTHENA (Berne, Switzerland) as previously described [11]. Three 6-week-old $Dmd^{EGFP\text{-}mdx}$ mice were injected intravenously into the retro-orbital sinus under general anaesthesia using 1.5%–2% isoflurane once a week with the tcDNA compound for an extended period of 20 weeks and at a dose of 200 mg/kg/week. *Intravital* imaging was done 1 week after the last injection as described below. The treated mice were killed 3 weeks following the last injection.

AAV-vector cloning

pAAV-SaCas9-sgRNA22 The *Staphylococcus aureus* Cas9 (saCas9)-3HA-U6-sgRNA scaffold cassette from the pX601 plasmid (Addgene 61591, Watertown, MA, USA) was cloned into an AAV-2 plasmid under the control of the C5.12 promoter. The target sequence TAC ACT AAC ACG CAT ATT TG [15] of intron 22 of the murine *Dmd* gene, was subsequently cloned 5′ of the sgRNA scaffold to obtain the plasmid pAAV-SaCas9-sgRNA22.

pAAV-Cherry-sgRNA23 The U6-sgRNA scaffold cassette from the pX601 plasmid (Addgene 61591) was cloned into an AAV-2 plasmid downstream of a C5.12 Strep Tag mCherry cassette. The target sequence CAT TGC ATC CAT GTC TGA CT [15] of intron 23 of the murine *Dmd* gene, was subsequently cloned 5′ of the sgRNA scaffold to obtain the plasmid pAAV-Cherry-sgRNA23.

AAV production

Adenovirus free rAAV2/9 viral preparations were generated by packaging AAV2-ITR recombinant genomes in AAV9 capsids, using a three plasmid transfection protocol as previously described [16]. Briefly, HEK293 cells were co-transfected with the pAAV-transgene (pAAV-SaCas9-sgRNA22 or pAAV-Cherry-sgRNA23), an AAV9 RepCap plasmid (pAAV2.9, Dr J. Wilson, UPenn) and an adenoviral helper plasmid (pXX6) at a ratio of 1:1:2. Crude viral lysate was harvested at 60 h posttransfection and lysed by freeze-and-thaw cycles. The viral lysate was purified through two rounds of CsCl ultracentrifugation followed by dialysis. Viral genomes were quantified by a TaqMan real-time PCR assay using primers and probes corresponding to the inverted terminal repeat region (ITR) of the AAV vector genome [17]. The primer pairs and TaqMan probes used for ITR amplification were as follows: 1AAV65/Fwd: 5′-CTC CAT CAC TAG GGG TTC CTT G-3′; 64AAV65/rev: 5′-GTA GAT AAG TAG CAT GGC-3′; and AAV65MGB/taq: 5′-TAG TTA ATG ATT AAC CC-3′.

50 µl containing both AAVs (*AAV-SaCas9-sgRNA22 and AAV-Cherry-sgRNA23)* at a titre of 4.6e10 vg of each were injected into the anterior muscle compartment of the lower leg of 6-week-old $Dmd^{EGFP\text{-}mdx}$ mice and killed 5 months post injection.

Intravital confocal and multiphoton scanning microscopy

Mice were anaesthetized with isoflurane. After one longitudinal incision of the skin at the lateral side of the lower hindlimb, the exposed muscle was stably positioned on a coverslip that was fixed to the sample holder, thereby minimizing motion artefacts and enabling high-resolution microscopy over several hours. Mice were kept at 37°C in the microscope's incubation chamber during the entire imaging procedure. Muscles were imaged with a combined confocal/multiphoton point-scanning microscope (SP8 MP-Leica microsystem, Wetzlar, Germany) equipped with a Ti: Sapphire femto-second laser (Mai Tai Deep see-Spectra Physics) allowing a tuning range for excitation between 690 and 1040 nm. A long-working distance 25x numerical aperture (NA) 0.95/water (Leica) lens was used for intravital deep sectioning up to 300 μm depth at 5–10 μm Z-step size. For the confocal imaging, EGFP was excited with a 488 nm laser line and the fluorescence was collected using classical photomultiplier detectors (PMT). Their spectral detection window was set between 496-546 nm. Multiphoton laser was used to excite EGFP with a wavelength of 900 nm during live-imaging. The emission photons where spectrally separated by a dichroic beam splitter (DM484) and collected on three nondescanned photomultiplier detectors (NDD-PMT), the band pass filter 500–550 nm was used for EGFP signal, the band pass filter 565-605 nm for mCherry signal and the band pass filter 625–675 nm was used to register the tissue autofluorescence signal. The 3D videos were obtained using Arivis Software.

Serum CPK analysis

Blood samples were collected from the facial vein of 8- to 10-month-old wild-type (C57BL/6N) and *Dmd*^EGFP-mdx^ mice. Serum creatine phosphokinase (CPK) levels were measured based on the quantification of NADPH formation derived from the action of CPK on creatine phosphate as recommended by the International Federation of Clinical Chemistry in an automated biochemistry analyser (AU680, Beckman Coulter, Brea, CA, USA) by the pathology laboratory at Mary Lyon Centre, Medical Research Council, Harwell, Oxfordshire, UK.

Western blot analyses

Total protein was extracted from cryo-sections of different skeletal muscles (*biceps brachii*, *tibialis anterior*, *triceps brachii*, *quadriceps*, *gastrocnemius* and diaphragm) and from cardiac muscle of 4-month-old wild-type *Dmd*^EGFP^ and *Dmd*^EGFP-mdx^ mice. Protein extracts were obtained from pooled muscle sections in RIPA buffer (25 mM Tris-HCl (pH 7.6), 150 mM NaCl, 1% NP-40, 1% sodium deoxycholate) with 5% SDS and 1x pierce protease inhibitor (Thermo Fisher, Waltham, MA, USA). Samples were denatured in 1x NuPAGE reducing agent (Thermo Fischer: NP0009) with 1x NuPAGE LDS Sample Buffer (Thermo Fischer: NP0008) at 100°C for 3 min. Total protein concentration was determined with BCA protein assay kit (Thermo Fisher) and 25 μg of proteins were loaded onto NuPAGE 3-8% TRIS-acetate protein gels (Invitrogen, Carlsbad, CA, USA) in 1x NuPAGE TRIS-acetate SDS Running Buffer (Thermo Fisher) following manufacturer's instructions.

Dystrophin protein was detected by probing the nitrocellulose membrane with the primary NCL-DYS1 mouse monoclonal antibody (1:130 dilution, NCL-DYS1; Novocastra, Leica Biosystems, Wetzlar, Germany). Vinculin as internal loading control was detected by the primary monoclonal anti-vinculin (mouse IgG1 isotype) antibody (1:10,000 dilution, Sigma Aldrich, St. Louis, MO, USA). EGFP protein was detected with a primary anti-GFP rabbit serum polyclonal antibody (1:700 dilution, Thermo Fisher). Incubations with primary antibodies were followed by incubation with a goat anti-mouse secondary antibody IRDye® 800CW (Li-Cor, Lincoln, NE, USA) for dystrophin and vinculin detection and with a goat anti-rabbit secondary antibody IRDye® 700CW (Li-Cor) for GFP, using the iBind Flex Western Device. Membrane fluorescence was converted to value images using the Odyssey® CLx imaging system (Li-cor). Band fluorescent densities were analysed using the Image Studio™ software (Li-cor). For the purpose of visual presentation of the infrared fluorescent protein bands we allocated green colour to visualize the signal from the goat anti-mouse secondary antibody IRDye® 800CW which bound to anti-dystrophin and anti-vinculin primary antibodies, and red colour to visualize the signal from the goat anti-rabbit secondary antibody IRDye® 700CW which bound to the anti-GFP primary antibody.

Histological analyses

Triceps brachii (Tri), tibialis anterior (TA) muscles, diaphragm, heart and *ileum* were harvested from 5- to 12-month-old Dmd^{EGFP} and $Dmd^{EGFP-mdx}$ mice. The tissues were mounted using either 6% Tragacanth gum 292 (Sigma-Aldrich) or OCT and snap-frozen in liquid nitrogen-cooled isopentane and stored at −80°C. The tissues were then processed for cryo-sectioning. 8–10 μm cross sections were collected and directly mounted with PBS for EGFP visualization or directly fixed with 4% PFA and stained. For imaging of innervating peripheral motor nerve branches, *EDL* muscles were dissected and directly fixed with 4% PFA; subsequently, smaller bundles were teased/peeled from the muscle and stained.

Immunohistological analyses were performed using primary antibodies against dystrophin (1:50 dilution, DYS2, mouse IgG1, Novocastra), CD31 (1:25 dilution, rabbit, Abcam, Cambridge, UK), MANDYS19 (1:10, mouse IgG1, DSHB, Iowa City, IO, USA), GFP (1:500, rabbit IgG, Thermo Fisher), β-tubulin III (1:500, mouse IgG2a, Sigma-Aldrich) and laminin (1:500, rabbit, Sigma-Aldrich), followed by incubation with fluorochrome-labelled secondary antibodies (1:400, ALEXA Fluor® goat anti-mouse IgG1-568, IgG2a-568 or IgG (H&L)-568 and goat anti-rabbit 488/647, Thermo Fisher) and mounted using Vectashield® Antifade Mounting Medium with DAPI (Vector Laboratories, Burlingame, CA, USA). For all sections incubated with mouse monoclonal antibodies an additional blocking step was performed: after fixation, sections were blocked with mouse IgG blocking solution from the M.O.M. kit (Vector Laboratories). Fluorescence was visualized using a Zeiss Axio Imager with an ORCA camera (Hamamatsu, Japan) and AxioVision software or images were recorded with an inverted fluorescent microscope (Leica DMI4000).

Confocal images were taken at the AMBIO facility at the Charité University Hospital, Berlin using a Nikon Scanning Confocal A1Rsi + system, with a 40x-Apo-DIC N2 λ S objective. Stacks (316.2 × 316.2 × 7.2 μm) of images 0.8 μm apart were captured at 1024 × 1024 pixel resolution. Images were analysed and displayed as videos using the Fiji software.

Haematoxylin–eosin staining was undertaken according to standard procedures, and the images were recorded using a digital slide scanner (Leica) and analysed with the ImageScope software.

Isolation of *EDL* single myofibres

Extensor digitorum longus (EDL) muscles were dissected and digested in 0.2% collagenase type I (Sigma-Aldrich) in FluoroBrite DMEM media (GIBCO, Thermo Fisher) supplemented with 1% penicillin/streptomycin, 4 mM L-glutamine (GIBCO) and 1% sodium pyruvate (GIBCO). Individual, viable and undamaged myofibres were isolated by gently passing them through Pasteur pipettes with different sized apertures as described in detail elsewhere [18]. The isolated living myofibres were either mounted on slides with PBS for direct EGFP-fluorescence detection or cultured for 40 h in the above mentioned isolation medium that was additionally supplemented with 10% horse serum (GIBCO) and 0.5% chicken embryo extract (MP Biomedicals, Santa Ana, CA, USA). Myofibres were viewed using SteReo Lumar.V12 stereoscope and Zeiss Axio Imager microscope equipped with an Orca® camera (Hamamatsu). AxioVision software was used for image acquisition.

Results

Generation and validation of the $Dmd^{EGFP-mdx}$ dystrophic reporter mouse model

For the generation of the $Dmd^{EGFP-mdx}$ mice, we used our previously characterized Dmd^{EGFP} mouse line that we crossed with the congenic Dmd^{mdx} mouse line on the C57BL/6N background. The female F1 mice were heterozygous for Dmd^{EGFP} and Dmd^{mdx} alleles. They were crossed with Dmd^{EGFP} males, and F2 males were screened for crossover events during meiosis that would recombine both alleles in *cis*. We had calculated this event to be present in 1:100 oocytes given the genetic distance of ≈1.1 Mbps between exons 23 and 79 of the *Dmd* gene (Figure 1A), which would equal ≈1 centiMorgan (cM). If the *mdx-23* nonsense mutation and the *EGFP*-tag are on the same allele, male mice will not express the EGFP-tag due to the intervening premature termination codon, at least not for the full-length muscle isoform. The *EGFP*-tag will be (re-) expressed if the reading frame of exon 79 is restored, such as observed in revertant fibres.

We obtained the first desired crossover in the 163rd animal. Further crosses between the *Dmd*^{EGFP-mdx} male and heterozygous females led to the establishment and expansion of a stable line of hemizygous male and homozygous female *Dmd*^{EGFP-mdx} mice (Figure 1B). The mice were genotyped for both the presence of the EGFP-sequence by triple oligonucleotide primer PCR (Figure 1) and for the *mdx-23* mutation by Sanger sequencing (Figure 1D). There was no significant difference in the postnatal viability until 21 days of age of the new *Dmd*^{EGFP-mdx} line in comparison to the wild-type *Dmd*^{EGFP} mice (Figure 1E). Since the generation of the mouse line, many mice lived until 24 months of age with no increased spontaneous death rate during ageing.

Western blot analysis confirmed the absence of full-length dystrophin-EGFP in protein lysates from *Dmd*^{EGFP-mdx} heart, diaphragm, as well as *biceps brachii*, *triceps brachii*, *quadriceps femoris*, *gastrocnemius* and *tibialis anterior* muscles. Expression of the full-length Dp427-EGFP isoform was present in positive controls from wild-type *Dmd*^{EGFP} muscle lysates (Figure 2A). Interestingly, Western blots of wild-type *Dmd*^{EGFP} muscle lysates revealed two separate bands when stained with anti-DYS1 antibody, whereas only the upper band was EGFP positive.

When performing histology, native dystrophin-EGFP-fluorescence was visible in fresh cryosections at the sarcolemma of *Dmd*^{EGFP} skeletal, heart and in smooth muscle of the *ileum*, but absent in *Dmd*^{EGFP-mdx} mice, except for sporadic revertant fibres (Figure 2B).

Skeletal muscle from adult *Dmd*^{EGFP-mdx} mice showed the same histopathological alterations as observed in dystrophic *Dmd*^{mdx} mice. These changes comprised increased variation of myofibre size, myofibre necrosis, internally positioned myonuclei, fatty replacement, mononuclear cell infiltrates, as well as fibrosis (Figure 2C). Serum levels of creatine phosphokinase were up to 20-fold elevated in *Dmd*^{EGFP-mdx} mice, thereby confirming the presence of muscular dystrophy (Figure 2D).
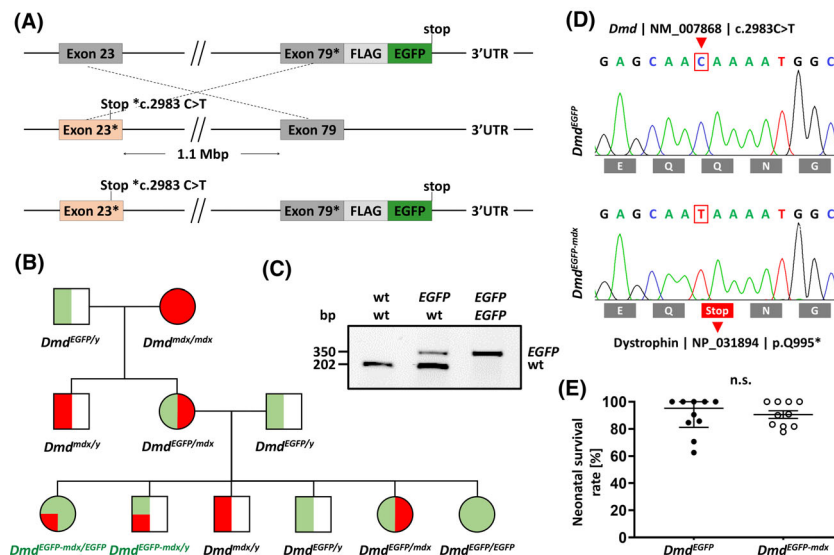
Figure 1. Generation and genotyping of the *Dmd*^{EGFP-mdx} reporter mouse line. **(A)** Scheme depicting the breeding programme to introduce the *Dmd*^{EGFP} allele into the *mdx* background in *cis* after natural recombination during meiosis in female F1 mice that are heterozygous for both alleles. The physical genomic distance between the *mdx-23* mutation and C-terminal EGFP tag is 1.1 Mbps corresponding to a recombination frequency of ≈1 centiMorgan (cM). Successful crossing-over could then be detected in the male progeny of the F2 generation (*Dmd*^{EGFP-mdx/y}). **(B)** Schematic pedigree with all possible genotypes illustrating the breeding strategy. Squares depict male, circles female animals. The *EGFP*-allele is depicted in green, the *mdx* allele in red. After successful crossing-over, expected to occur in ≈1:100 progeny from the F2 generation, further breeding with *Dmd*^{EGFP-mdx/y} males and *Dmd*^{EGFP-mdx/EGFP} females and subsequent genotyping resulted in a *mdx-EGFP* line starting from F4. **(C)** PCR genotyping for the *EGFP* sequence using a three oligonucleotide primer PCR. The presence of the *EGFP* sequence results in a 350 bp band, and its absence in a 202 bp band. Homo/hemizygous animals can be easily distinguished from heterozygous ones. **(D)** Sanger sequencing for the *mdx* mutation leading to a premature TAA termination codon at p.Q995 of the dystrophin protein. **(E)** The viability of *Dmd*^{EGFP-mdx} neonates, before weaning (21 days) was compared to wild-type *Dmd*^{EGFP} mice. Values are depicted as dot-plots with interquartile range, the difference of the survival rate was not significant, $P = 0.8304$ ($n = 10$ breeding cages, two-tailed, nonparametric Mann–Whitney U-test). [Colour figure can be viewed at wileyonlinelibrary.com]

## Revertant dystrophin-EGFP co-localizes with anti-dystrophin immunostaining

Revertant myofibres expressing native dystrophin-EGFP were easily identified by epifluorescence microscopy after cross-sectioning (Figure 3). For this, a coverslip was mounted on the slide using a drop of PBS, allowing microscopic inspection immediately after sectioning. Dystrophin-EGFP-negative myofibres were invisible when fluorescence intensities of revertant myofibres were set at comparable levels to those of myofibres from wild-type Dmd^{EGFP} mice. Furthermore, we compared dystrophin-EGFP fluorescence intensity of the identical revertant myofibre clusters before and after immunostaining (Figure 3). The native dystrophin-EGFP-fluorescence of revertant myofibres decreased only slightly during subsequent immunostaining steps and co-localized exactly with the signals from anti-dystrophin and anti-laminin staining, thereby confirming the presence of revertant dystrophin (Figure 3).

Expression of non-muscle dystrophin-EGFP isoforms

Moreover, we analysed the expression of shorter dystrophin-EGFP isoforms in non-muscle tissues, which should have remained unaffected as their initiation codons are located downstream of the *mdx*-23 mutation. Indeed, we detected strong native EGFP-fluorescence corresponding to the Dp71 isoform in the cerebral blood vessels, expressing CD31 (Figure S1A). However, we did not detect any native EGFP-fluorescence in neurons (data not shown).

We previously demonstrated that retina from wild-type Dmd^{EGFP} mice expressed full-length Dp427 as well
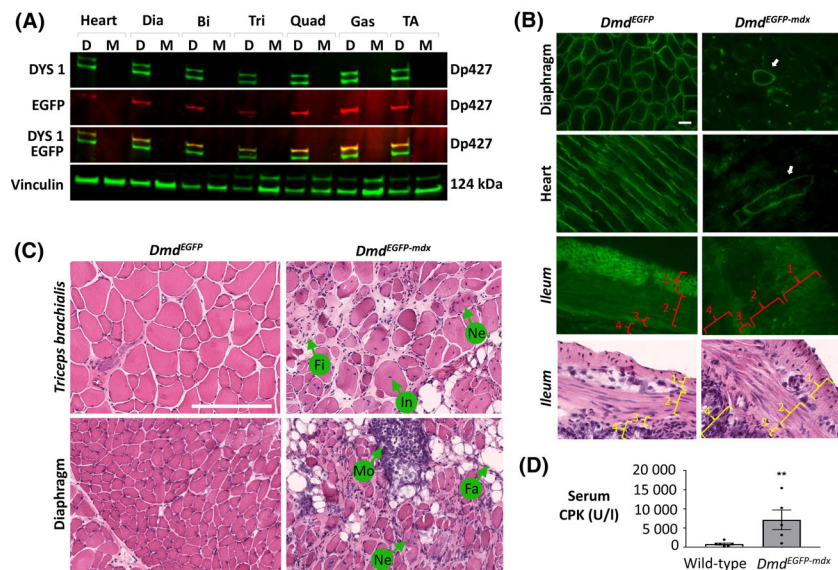
Figure 2. Characterization of the $Dmd^{EGFP-mdx}$ mouse. The $Dmd^{EGFP-mdx}$ mouse, like the *mdx* mouse, does not express Dp427 and develops a muscular dystrophy. **(A)** Western blot analysis of protein extracts from heart, diaphragm (Dia), *biceps brachii (Bi)*, *triceps brachii (Tri)*, *quadriceps femoris (Quad)*, *gastrocnemius (Gas)* and *tibialis anterior (TA)* muscles using DYS1 anti-dystrophin antibody against the rod domain, anti-GFP antibody and anti-vinculin antibody as internal loading control. Two secondary antibodies labelled with near-infrared dyes were used and for the purpose of visual presentation of the infrared fluorescent protein bands, we allocated green colour to visualize dystrophin and vinculin bands and red colour to visualize the EGFP-Dp427 band. The full-length Dp427 isoform was present in Dmd^{EGFP} *(D)* and wild-type muscle and absent in $Dmd^{EGFP-mdx}$*(M)* muscle. The anti-GFP antibody (in red) detected the tagged Dp427-EGFP protein only in Dmd^{EGFP} muscle and co-localized only with the upper band of the two separate bands obtained with the Dys1 antibody (in green). **(B)** Unstained cross-sections of skeletal, cardiac and smooth muscles revealed native EGFP-fluorescence (green) in Dmd^{EGFP} mice, but not in $Dmd^{EGFP-mdx}$ mice. A single revertant myofibre expressing native dystrophin-EGFP can be seen on the image of the diaphragm and heart (arrow). *Ileum* was also shown following Haematoxylin-Eosin (HE) staining. Layers: 1 – *muscularis externa*, 2 – *muscularis interna*, 3 – *muscularis mucosa/submucosa*, 4 – *mucosa*. Scale bar: 20 μm. **(C)** HE staining of *triceps brachialis* muscle and *diaphragm* cross-sections of 5-month-old $Dmd^{EGFP-mdx}$ mice showed signs of the presence of muscular dystrophy, such as internalized myonuclei (In), necrosis (Ne), mononuclear cell infiltration (Mo), fatty degeneration (Fa) and fibrosis (Fi) in comparison to age-matched Dmd^{EGFP} controls. Scale bar: 200 μm. **(D)** Serum creatine phosphokinase (CPK) activities were pathologically increased in sera from $Dmd^{EGFP-mdx}$ mice ($n = 5$, 9-to 13-month-old mice) as compared to wild-type mice ($n = 6$, 8- to 10-month-old mice). Values are depicted as dot-plots with mean ± SEM, the difference was significant with $P < 0.01$ (two-tailed, nonparametric Mann–Whitney U-test). [Colour figure can be viewed at wileyonlinelibrary.com]

as the retina-specific Dp260 dystrophin isoforms at the photoreceptor terminals [13]. Dp427 can be detected specifically using the anti-dystrophin antibody MAN-DYS19, which recognizes an epitope encoded by exon 21 that is located N-terminally of the premature termination codon of exon 23. In wild-type *Dmd*^{EGFP} mice, we observed strong native EGFP-fluorescence at the photoreceptor terminals of the retina that co-localized with the signal obtained by immunofluorescence using the MAN-DYS19 antibody and which corresponds to Dp427 isoform (Figure S1B). In *Dmd*$^{EGFP-mdx}$ mice, however, we did not detect full-length Dp427 at the photoreceptor terminals using MANDYS19 antibodies, whereas a native EGFP-signal was still present, corresponding to the Dp260 retina-specific isoform (Figure S1B).

Dp116 is a Schwann cell-specific isoform encoded by *Dmd* exons 56–79 [19]. We confirmed the presence of Dp116 expression in *Dmd*$^{EGFP-mdx}$ mice following co-immunostaining of a peripheral motor nerve branch and in a transverse section of the sciatic nerve using an anti-GFP antibody for signal enhancement along with β-tubulin III as neuronal marker (Figure S2A, B, Videos S1 and S2).

Live-imaging of sarcolemmal dystrophin-EGFP

Intravital microscopy of the lateral part of *tibialis anterior* (*TA*) muscle in anaesthetized *Dmd*^{EGFP} mice revealed homogeneous dystrophin-EGFP expression at the sarcolemma (Figure 4A, Video S3). In *Dmd*$^{EGFP-mdx}$ mice, only dot-like autofluorescent structures were visible at different emission wavelengths, likely corresponding to macrophages, whereas sarcolemmal dystrophin-EGFP was entirely absent (Figure S3A, B and Video S4). Occasionally, we found dystrophin-EGFP-expression in single myofibres or in small fibre clusters (Figure 4D). The dystrophin-EGFP-signal was present along smaller or larger segments of these fibres at the sarcolemma thus qualifying them as being 'revertant'.

Next, we isolated whole myofibres from the *extensor digitorum longus* (*EDL*) muscles of adult wild-type C57BL6, *Dmd*^{EGFP} and *Dmd*$^{EGFP-mdx}$ mice. Living myofibres from wild-type mice and *Dmd*$^{EGFP-mdx}$ mice did not show any fluorescence (Figure S3C–F), whereas myofibres from *Dmd*^{EGFP} mice expressed dystrophin-EGFP homogeneously along the sarcolemma (Figure 4B). Revertant myofibres from *Dmd*$^{EGFP-mdx}$ mice were detectable under the binocular microscope by their green fluorescence and could be isolated for subsequent live-imaging experiments using higher resolution microscopy or for subsequent myofibre culture (Figure 4E and Figure 3G,H). We next cultured single myofibres from *Dmd*^{EGFP} and revertant myofibres from *Dmd*$^{EGFP-mdx}$ mice and demonstrated that dystrophin-EGFP-expression persisted at the sarcolemmal position after 2 days in culture (Figure 4C,F).
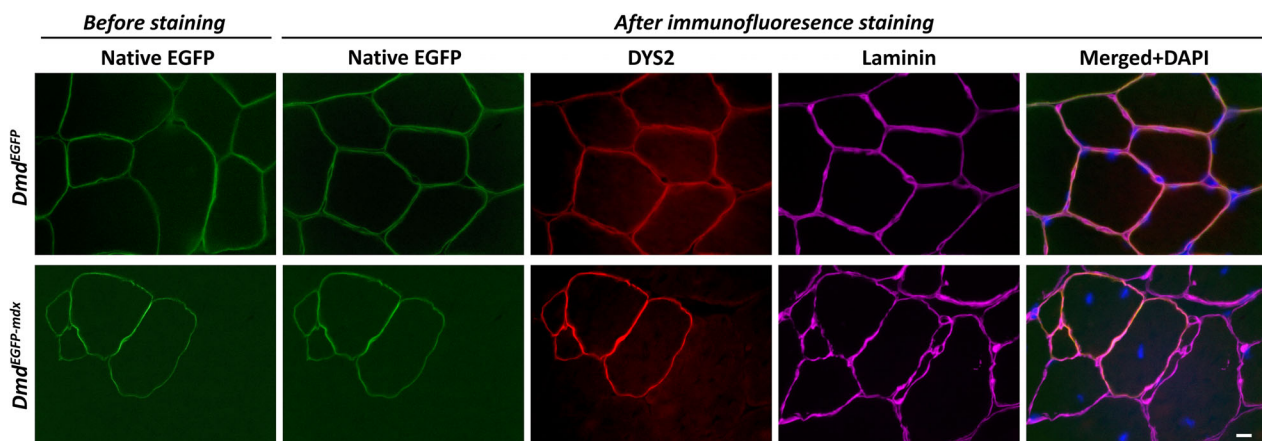

Figure 3. Revertant dystrophin-EGFP co-localizes with the anti-dystrophin immunosignal. Cross sections of the *tibialis anterior* muscle from *Dmd*$^{EGFP-mdx}$ mice showing dystrophin-EGFP expression at the level of the sarcolemma of a revertant myofibre cluster before and after immunostaining. We stained serial sections from the same region of interest with antibodies against the C-terminal dystrophin domain (DYS2, red) in conjunction with laminin, a basement membrane protein (magenta). We observed exact co-localization between the native dystrophin-EGFP-fluorescence and the anti-dystrophin immunosignal. Merged images additionally depict the nuclei stained with DAPI (blue). Native dystrophin-EGFP-fluorescence does not fade during subsequent immunostaining procedures. Scale bar: 10 μm. [Colour figure can be viewed at wileyonlinelibrary.com]

Live-imaging of therapeutically restored dystrophin

In order to evaluate the efficacy of our mouse model for evaluating dystrophin restoration we performed two different therapeutic approaches. For the first approach, we targeted the RNA of dystrophin, by systemically treated adult *Dmd*^{EGFP-mdx} mice with weekly doses of 200 mg/kg tcDNA to induce *Dmd* exon-23 skipping, as previously published [11]. Following 20 weeks of tcDNA treatment, dystrophin-EGFP was restored along the entire sarcolemma of all myofibres as revealed by intravital microscopy, whereas less autofluorescent
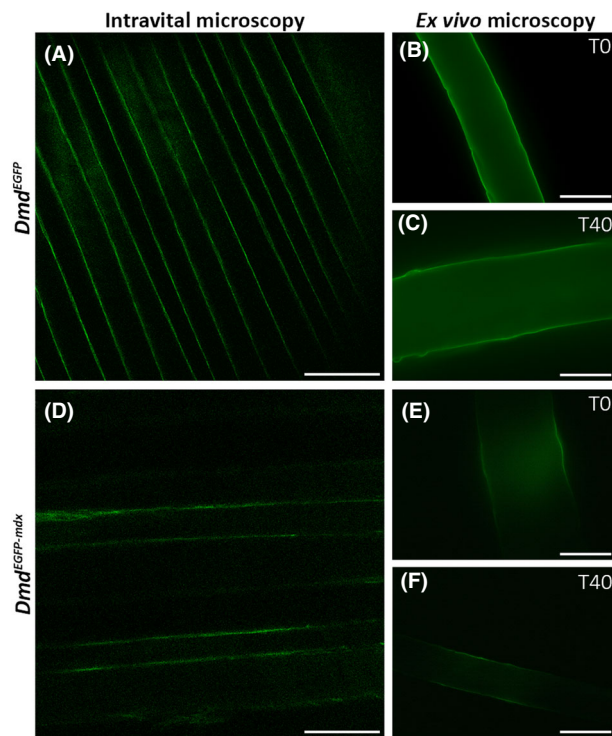
Figure 4. Live-imaging of sarcolemmal dystrophin-EGFP. **(A)** Confocal intravital microscopy of *Dmd*^{EGFP} *tibialis anterior* muscle revealed homogeneous fluorescence of dystrophin-EGFP protein at the sarcolemma of superficial myofibres. Scale bar: 100 μm. **(B–C)** Isolated myofibres from *Dmd*^{EGFP} EDL muscle. Native dystrophin-EGFP was homogeneously expressed along the sarcolemma when live-imaged by epifluorescence microscopy directly after isolation (T0; image **B**) or after 40 h in culture (T40; image **C**). Scale bar: 50 μm. **(D)** Confocal intravital microscopy of *Dmd*^{EGFP-mdx} *tibialis anterior* muscle revealed patchy dystrophin-EGFP expression at the sarcolemma of two revertant myofibres. Revertant dystrophin-EGFP was not expressed homogeneously, but in a segmental fashion. Scale bar: 100 μm. **(E–F)** Isolated revertant myofibres from *Dmd*^{EGFP-mdx} EDL muscle. Native dystrophin-EGFP was expressed along the sarcolemma of a short revertant myofibre segment when viewed using epifluorescence microscopy directly after isolation (T0; image **E**) or after 40 h in culture (T40; image **F**). Scale bar: 50 μm. [Colour figure can be viewed at wileyonlinelibrary.com]

macrophages were visible (Figure 5A and Video S5). In the second therapeutic approach, we targeted the DNA by injecting AAV-SaCas9-sgRNA22 combined with AAV-Cherry-sgRNA23 vectors into the anterior muscle compartment of lower legs of adult *Dmd*^{EGFP-mdx} mice to induce *Dmd* exon-23 excision. Five months following AAV injection, a large number of myofibres expressed mCherry in the cytoplasm, demonstrating successful transduction of many myofibres (Figure 5C'). Dystrophin was found only in short sarcolemmal segments of these mCherry-positive myofibres, suggesting that exon 23 excision occurred only in a small percentage of myonuclei, thereby preventing widespread dystrophin restoration (Figure 5C).

Moreover, we isolated whole myofibres from the *extensor digitorum longus* (EDL) muscles of *Dmd*^{EGFP-mdx} mice following tcDNA or AAV treatment. As expected from intravital imaging, single myofibres from tcDNA-treated mice expressed widespread dystrophin-EGFP along the sarcolemma (Figure 5B), whereas AAV-treated myofibres expressed dystrophin-EGFP only in short segments (Figure 5D–D').

Discussion

Here we describe the generation, the phenotype and the experimental usefulness of the first dystrophin-EGFP reporter mouse in the *mdx* context, which we named *Dmd*^{EGFP-mdx} mouse.

We designed the *Dmd*^{EGFP-mdx} mice by introducing an EGFP-coding sequence fused in-frame to *Dmd* exon 79 into the *mdx*-23 allele, which harbours a nonsense mutation in exon 23. *Dmd*^{EGFP-mdx} mice developed the identical muscular dystrophy phenotype as ordinary *mdx* mice as evidenced by the presence of typical histopathological hallmarks and increased serum CPK levels. The presence of the *mdx*-23 mutation resulted in the absence of full-length Dp427 dystrophin in skeletal, heart and smooth muscle. Importantly, we observed sporadic revertant myofibres and revertant fibre clusters, both in skeletal and heart muscle. Those fibres expressed the dystrophin-EGFP fusion protein at the expected subsarcolemmal location. We were also able to detect the expression of the shorter dystrophin isoforms in the retina (Dp260), in the peripheral nerve (Dp116) and in the brain (Dp71), which are all unaffected by the *mdx*-23 mutation.

We demonstrated that dystrophin-EGFP could be restored at its sarcolemmal position by therapeutic
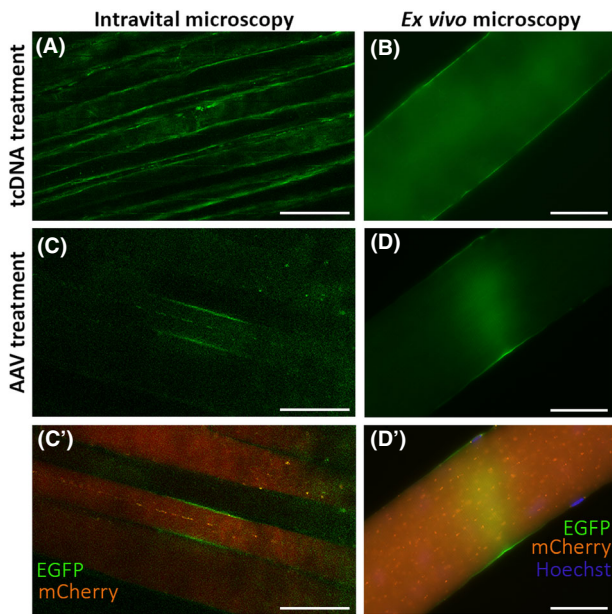
Figure 5. Live-imaging of therapeutically restored dystrophin. **(A)** *Dmd*^EGFP-mdx mice were systemically treated for 5 months with 200 mg/kg/week tcDNA. Multiphoton intravital microscopy of *TA* muscle revealed homogeneous restoration of dystrophin-EGFP protein at the sarcolemma of superficial myofibres. N = 3. Scale bar: 100 μm. **(B)** Isolated myofibre from *EDL* muscle from tcDNA-treated *Dmd*^EGFP-mdx mice. Native dystrophin-EGFP was seen to be expressed along the sarcolemma by live-imaging using epifluorescence microscopy directly after isolation. N>20. Scale bar: 50 μm. **(C and C')** Anterior muscle compartment of the lower leg of *Dmd*^EGFP-mdx mice was injected with AAV-SaCas9-sgRNA22 along with AAV-Cherry-sgRNA23 vectors. Confocal intravital microscopy of *TA* muscle was performed after 5 months of transduction. Restoration of dystrophin-EGFP was found in short segments of transduced myofibres. Successful transduction of myofibres with AAV-Cherry-sgRNA23 was revealed by cytoplasmic mCherry fluorescence. N = 5. Scale bar: 100 μm. **(D and D')** Isolated myofibre of *EDL* muscle from AAV injected mice was live-imaged using epifluorescence microscopy directly after isolation. Native fluorescence of restored sarcolemmal dystrophin-EGFP was found in a short fibre segment, whereas mCherry was expressed throughout the cytoplasm. Hoechst showing myonuclei. N>20. Scale bar: 50 μm. [Colour figure can be viewed at wileyonlinelibrary.com]

modulation of splicing as well as by genome editing, thereby confirming previous results in classical *Dmd*^mdx mice [11,15]. We achieved widespread restoration of dystrophin following tcDNA-induced exon 23 skipping, whereas dystrophin expression was patchy following AAV induced exon 23 excision. It should be noted, however, that we here injected relatively low viral titres of slightly different AAV constructs as compared to previously published data [15], which may be the reason for the failure to achieve widespread dystrophin restoration.

We succeeded in visualizing dystrophin in living skeletal muscle without antibody staining at the correct subcellular position *in vivo* as well as *ex vivo*. During intravital microscopy, dystrophin-EGFP-fluorescence persisted without much photobleaching for at least 1 hour in anaesthetized mice. Muscle could be imaged for up to a depth of 150 μm maximum following cutaneous incision and by leaving the muscle fascia intact. At the end of imaging and after cutaneous suture, mice recovered rapidly and could be kept for further experiments. Our future goal is to develop live pharmacodynamics for dystrophin restoration therapies. For this, we are currently developing a transcutaneous window allowing repetitive live-imaging of skeletal muscle for up to several weeks, similarly as co-authors of this work recently developed for tumour imaging [20]. Such longitudinal observations are essential to determine dosages and dosage intervals for long-term treatment protocols. Such a study protocol could also drastically reduce the number of required animals according to the 3R principles of Russell & Burch [21].

We also showed that fluorescence of sarcolemmal dystrophin-EGFP was maintained during culture of isolated myofibres for up to 2 days. We are currently testing the maximum duration of such cultures and we are developing a protocol for time-lapse imaging of individual fibres at specific subcellular positions.

Dmd^EGFP-mdx mice bear some additional advantages over classical *mdx* mice for research on dystrophin expression. Their use makes immunohistological processing redundant, allowing fast sample processing, avoiding antibody related signal amplification artifacts as well as avoiding antibody induced nonspecific background staining, often being present in inflamed *mdx* muscle. Of note, nonspecific background staining can be reduced using specific blocking protocols or using anti-dystrophin antibodies produced in other species than mice.

Disadvantageous is the autofluorescence following oxidation of the EGFP signal, which, however, only appears after prolonged storage at air oxygen levels before fixation of the material. We found that rapid tissue processing and immediate viewing after cryo-sectioning yielded best results.

We previously demonstrated the presence of two separate bands at the position of Dp427 full-length dystrophin in Western blots from wild-type and from *Dmd*^EGFP muscle [13], a result that we herein

reproduced. Although both bands were positive for DYS1 antibody staining (directed against the rod domain), only the upper and more slowly migrating band was also positive for H4 antibody staining (directed against the C-terminus) and EGFP. This suggests the presence of an alternatively spliced isoform at the C-terminus along with the full-length isoform, which now becomes further separated due to the larger molecular weight of the dystrophin-EGFP fusion protein.

In conclusion, we show that the $Dmd^{EGFP-mdx}$ mouse is a very useful model due to its potential applications for live kinetic and quantitative analyses of spontaneously or therapeutically restored dystrophin expression *in vivo* and *ex vivo*.

Ethics approval and consent to participate

The animal (mouse) experiments were approved by the LaGeSo Berlin (Registration number T 0222/13) and by the French government (Ministère de l'Enseignement Supérieur et de la Recherche, autorisation APAFiS).

Consent for publication

All authors have seen the final version of the manuscript and consented to its submission to Neuropathology and Applied Neurobiology.

Acknowledgements

Authors' contributions

MVP, AS, HA and MS designed the study. MVP, SMG and FS performed the molecular genetic experiments. MVP and MS supervised the breeding program. AS and OP performed the Western blot experiments. MVP and AS performed the histological analysis. MVP, AS, CLB and TM performed intravital confocal and multiphoton imaging. AS, AM, MVP and HA performed the single myofibre experiments. AG and LG designed the tcDNA. JBD and IR designed and produced AAV vectors. MVP, AS and HA wrote the first draft of the manuscript. MVP, HA and MS provided funding. All authors read the final version of the manuscript and gave their permission for publication.

Competing interests

The authors do not state any financial nor nonfinancial competing interests.

Funding

Data Availability Statement

All data generated or analysed during this study are included in this published article.

The data that support the findings of this study are openly available in [repository name e.g "figshare"] at http://doi.org/10.1111/nan.12639, reference number [reference number]

References

1 Hoffman E.P., Brown R.H. Jr, Kunkel L.M.. Dystrophin: The protein product of the duchenne muscular dystrophy locus. *Cell* 1987; **51**: 919–28. https://doi.org/10.1016/0092-8674(87)90579-4

2 Cox G.A., Phelps S.F., Chapman V.M., Chamberlain J.S.. New mdx mutation disrupts expression of muscle and nonmuscle isoforms of dystrophin. *Nat Genet* 1993; **4**: 87–93. https://doi.org/10.1038/ng0593-87

3 Vaillend C., Billard J.M., Claudepierre T., Rendon A., Dutar P., Ungerer A.. Spatial discrimination learning and CA1 hippocampal synaptic plasticity in mdx and mdx3cv mice lacking dystrophin gene products. *Neuroscience* 1998; **86**: 53–66

4 Hnia K., Hugon G., Masmoudi A., Mercier J., Rivier F., Mornet D.. Effect of beta-dystroglycan processing on

utrophin/Dp116 anchorage in normal and mdx mouse Schwann cell membrane. *Neuroscience* 2006; **141**: 607–20. https://doi.org/10.1016/j.neuroscience.2006.04.043

5 D'Souza V.N., Man N.T., Morris G.E., Karges W., Pillers D.-A., Ray P.N. A novel dystrophin isoform is required for normal retinal electrophysiology. *Hum Mol Genet* 1995; **4**: 837–42

6 Dunckley M.G., Manoharan M., Villiet P., Eperon I.C., Dickson G.. Modification of splicing in the dystrophin gene in cultured Mdx muscle cells by antisense oligoribonucleotides. *Hum Mol Genet.* 1998; **7**: 1083–1090

7 Long C., McAnally J.R., Shelton J.M., Mireault A.A., Bassel-Duby R., Olson E.N.. Prevention of muscular dystrophy in mice by CRISPR/Cas9-mediated editing of germline DNA. *Science* 2014; **345**: 1184–88. https://doi.org/10.1126/science.1254445

8 Lu Q.L., Mann C.J., Bou-Gharios G., Morris G.E., Xue S.A., Fletcher S. et al Functional amounts of dystrophin produced by skipping the mutated exon in the mdx dystrophic mouse. *Nat Med* 2003; **9**: 1009–14

9 Lu Q.L., Morris G.E., Wilton S.D., Ly T., Artem'yeva O.V., Strong P. et al Massive idiosyncratic exon skipping corrects the nonsense mutation in dystrophic mouse muscle and produces functional revertant fibers by clonal expansion. *J Cell Biol.* 2000; **148**: 985–96. https://doi.org/10.1083/jcb.148.5.985

10 Wilton S.D., Dye D.E., Blechynden L.M., Laing N.G.. Revertant fibres: a possible genetic therapy for Duchenne muscular dystrophy? *Neuromuscul Disord* 1997; **7**: 329–35

11 Goyenvalle A., Griffith G., Babbs A., El Andaloussi S., Ezzat K., Avril A. et al Functional correction in mouse models of muscular dystrophy using exon-skipping tricyclo-DNA oligomers. *Nat Med* 2015; **21**: 270–75. https://doi.org/10.1038/nm.3765

12 Shieh P.B.. Emerging strategies in the treatment of duchenne muscular dystrophy. *Neurotherapeutics.* 2018; **15**: 840–48. https://doi.org/10.1007/s13311-018-00687-z

13 Petkova M.V., Morales-Gonzales S., Relizani K., Gill E., Seifert F., Radke J. et al Characterization of a DmdEGFP reporter mouse as a tool to investigate dystrophin expression. *Skelet Muscle* 2016; **6**: 25. https://doi.org/10.1186/s13395-016-0095-5

14 Bulfield G., Siller W.G., Wight P.A., Moore K.J.. X chromosome-linked muscular dystrophy (mdx) in the mouse. *Proc Natl Acad Sci* 1984; **81**: 1189–92

15 Nelson C.E., Hakim C.H., Ousterout D.G., Thakore P.I., Moreb E.A., Castellanos Rivera R.M. et al In vivo genome editing improves muscle function in a mouse model of Duchenne muscular dystrophy. *Science* 2016; **351**: 403–07. https://doi.org/10.1126/science.aad5143

16 Bartoli M., Poupiot J., Goyenvalle A., Perez N., Garcia L., Danos O. et al Noninvasive monitoring of therapeutic gene transfer in animal models of muscular dystrophies. *Gene Ther* 2006; **13**: 20–8. https://doi.org/10.1038/sj.gt.3302594

17 Rohr U.-P., Wulf M.-A., Stahn S., Steidl U., Haas R., Kronenwett R.. Fast and reliable titration of recombinant adeno-associated virus type-2 using quantitative real-time PCR. *J Virol Methods* 2002; **106**: 81–8. https://doi.org/10.1016/s0166-0934(02)00138-6

18 Moyle L.A., Zammit P.S.. Isolation, culture and immunostaining of skeletal muscle fibres to study myogenic progression in satellite cells. *Methods Mol Biol* 2014; **1210**: 63–78. https://doi.org/10.1007/978-1-4939-1435-7_6

19 Matsuo M., Awano H., Matsumoto M., Nagai M., Kawaguchi T., Zhang Z. et al Dystrophin Dp116: a yet to be investigated product of the duchenne muscular dystrophy gene. *Genes.* 2017; **8**: 251. https://doi.org/10.3390/genes8100251

20 Rouffiac V., Roux KS.-L., Salomé-Desnoulez S., Leguerney I., Ginefri J.-C., Sébrié C. et al Multimodal imaging for tumour characterization from micro- to macroscopic level using a newly developed dorsal chamber designed for long-term follow-up. *J Biophotonics* 2020; **13**: e201900217. https://doi.org/10.1002/jbio.201900217

21 Tannenbaum J., Bennett B.T.. Russell and Burch's 3Rs then and now: the need for clarity in definition and purpose. *J Am Assoc Lab Anim Sci* 2015; **54**: 120–32

Supporting information

Additional Supporting Information may be found in the online version of this article at the publisher's web-site:

Figure S1. Detection of the dystrophin isoforms Dp71 and Dp260 in *Dmd*^{EGFP-mdx} mice. (A) The left image depicts a brain cross-section emitting native EGFP-fluorescence (green). Scale bar: 100μm. A higher magnification of a brain blood vessel (green) shows partial co-localization of the Dp71 EGFP-positive isoform with the endothelial cell marker CD31 (red). Scale bar: 10 μm. **(B)** Wild-type *Dmd*^{EGFP} retina was labelled with a MAN-DYS19 antibody to visualize full-length dystrophin in photoreceptor terminals. The MANDYS19 signal (red) and the native fluorescence of the dystrophin-EGFP fusion protein (green) co-localized at the same photoreceptor terminals (yellow), whereas the Dp260 isoform corresponds to the EGFP-only signal. The lower three images depict the retina from *Dmd*^{EGFP-mdx} mice. The MANDYS19 signal is absent, whereas the native EGFP-fluorescence persisted, corresponding to the Dp260 retinal isoform. Right images depict a magnified section of the adjacent image. Scale bar: 10 μm.

Figure S2. Detection of the dystrophin isoform Dp116 in *Dmd*^{EGFP-mdx} mice. **(A)** The confocal microscopy images (one representative image from the Z-stack) depict a bundle of myofibres from *Dmd*^{EGFP-mdx} EDL muscle together with their innervating peripheral motor nerve branch. The double immunolabelling with anti-GFP (green) and anti-β-tubulin III antibodies (red) reveals co-expression of Dp116 and β-tubulin III at peripheral motor nerve branches (yellow). The striation of skeletal muscle fibres is visible with Nomarski imaging (grey). **(B)** Staining of a sciatic nerve cross section with anti-GFP (green) and anti-β-tubulin III (red) confirms the expression of Dp116 in the peripheral nerve. β-Tubulin III expression can be observed in the central neurofilaments that are surrounded by the Dp116 signal from the Schwann's cells. The right image depicts a magnified section of the adjacent image. Scale bar: 100 μm.

Figure S3. Live-imaging of therapeutically restored dystrophin. **(A,B)** Intravital multiphoton microscopy of *TA* muscle from control *Dmd*^{EGFP-mdx} mice using a 500–550 nm band pass filter did not reveal any sarcolemmal dystrophin-EGFP-fluorescence **(A)**. Only dot-like structures were visible, which were also visible using the 625-675 nm band pass filter **(B)**, thus qualifying them as autofluorescent signals, likely originating from inflammatory cell infiltrates that are characteristic of dystrophic muscle. Scale bar: 200 μm. **(C,D)** Isolated myofibre from *EDL* muscle from wild-type C57BL6 mice did not show any signal in the GFP channel under live-imaging using epifluorescence microscopy directly after isolation, whereas the myofibre was visible with Nomarski imaging. Scale bar: 50 μm. **(E,F)** Isolated myofibre of *EDL* muscle from control *Dmd*^{EGFP-mdx} mice did not show any signal in the GFP channel under live-imaging using epifluorescence microscopy directly after isolation (applying same imaging parameters as for *Dmd*^{EGFP} myofibres), whereas the myofibre was visible with Nomarski imaging. N> 20. Scale bar: 50 μm. **(G,F)** Floating isolated myofibres of *EDL* muscle from control *Dmd*^{EGFP-mdx} mice were live imaged using a stereomicroscope immediately after isolation. EGFP-fluorescence of revertant fibre segments was easily detectable, whereas the nonrevertant fibre was only visible by dark-field microscopy.

Videos S1. The videos are the recordings of two confocal microscopy stacks of bundles of myofibres from *Dmd*^{EGFP-mdx} EDL muscle together with their innervating peripheral motor nerve branches. The double immunolabelling with anti-GFP (green) and anti-β-tubulin III antibodies (red) confirms co-expression of Dp116 and β-tubulin III in the peripheral motor nerve (yellow). The striation of skeletal muscle fibres is visible in the images recorded by Nomarski imaging in grey.

Videos S2. The videos are the recordings of two confocal microscopy stacks of bundles of myofibres from *Dmd*^{EGFP-mdx} EDL muscle together with their innervating peripheral motor nerve branches. The double immunolabelling with anti-GFP (green) and anti-β-tubulin III antibodies (red) confirms co-expression of Dp116 and β-tubulin III in the peripheral motor nerve (yellow). The striation of skeletal muscle fibres is visible in the images recorded by Nomarski imaging in grey.

Video S3. 3D-volume representation of a multiphoton scanning image stack from a wild-type *Dmd*^{EGFP} mouse. The mouse was anaesthetized and the lateral aspect of the lower leg muscles was imaged *in vivo*. Native dystrophin-EGFP-expression can be observed along the sarcolemma of the muscle fibres.

Video S4. 3D-volume representation of a multiphoton scanning image stack from a *Dmd*^{EGFP-mdx} mouse. The mouse was anaesthetized and the lateral aspect of the lower leg muscles was imaged *in vivo*. Native dystrophin-EGFP-fluorescence was absent at the sarcolemmal level of the muscle fibres. However, green fluorescent signals appeared as scattered spots. These spots were positive for red fluorescence as well, thereby qualifying them as autofluorescence (see green/red overlay at the end of the video). Most likely the signal represents macrophages, which are known to be autofluorescent and abundant in the *mdx* dystrophic muscle.

Video S5. 3D-volume representation of a multiphoton scanning image stack from a dystrophic *Dmd*^{EGFP-mdx} mouse treated with tcDNA for 20 weeks. The mouse was anaesthetized and the lateral aspect of the lower leg muscles were imaged *in vivo*. Restoration of native dystrophin-EGFP was be observed at the sarcolemma. Autofluorescent cells were less abundant (green, red and yellow overlay signal at the end of the video) than in *Dmd*^{EGFP-mdx} control mice (for comparison see **video 4**).